

## † Supporting Information

# Achieving Electronic Structure Reconfiguration in Metallic Carbides for Robust Electrochemical Water Splitting

*Lulu Qiao*<sup>a,1</sup>, *Anquan Zhu*<sup>a,1</sup>, *Weixuan Zeng*<sup>a</sup>, *Rui Dong*<sup>a</sup>, *Pengfei Tan*<sup>a</sup>, *Zhengping Ding*<sup>c,d</sup>, *Peng Gao*<sup>c,d,e</sup>, *Shuangyin Wang*<sup>b,\*</sup> and *Jun Pan*<sup>a,\*</sup>

<sup>a</sup> *State Key Laboratory for Powder Metallurgy, Central South University, Changsha 410083, P. R. China*

<sup>b</sup> *State Key Laboratory of Chem/Bio-Sensing and Chemometrics, College of Chemistry and Chemical Engineering, Hunan University, Changsha, Hunan, 410082, P. R. China.*

<sup>c</sup> *International Center for Quantum Materials, School of Physics, Peking University, Beijing 100871, China.*

<sup>d</sup> *Electron Microscopy Laboratory, School of Physics, Peking University, Beijing 100871, China.*

<sup>e</sup> *Collaborative Innovation Center of Quantum Matter, Beijing 100871, China.*

<sup>1</sup> *These authors contributed to this work equally*

\*Corresponding Author: [jun.pan@csu.edu.cn](mailto:jun.pan@csu.edu.cn)

[shuangyinwang@hnu.edu.cn](mailto:shuangyinwang@hnu.edu.cn)

## 1. *Characterizations*

The phase compositions of samples were validated by X-ray diffractometer (XRD, D/max 2550, Rigaku Corporation, Cu-K $\alpha$  radiation,  $\lambda=0.15405$  nm). Microstructures were observed by field emission scanning electron microscope (FE-SEM, Nova Nano SEM 230, FEI Co., Ltd.) and transmission electron microscopy (TEM, JEM-2100F, Japanese electronics Co., Ltd. and FEI Tecnai G2 F20 at 200kV with an Oneview IS (Gatan) camera and Oxford X-maxN TSR EDS detector). The surface element states and chemical composition were performed by the X-ray photoelectron spectroscopy (XPS, ESCALAB 250Xi ThermoFisher-VG, Mg-K $\alpha$  radiation), and the binding energy of all the elements was calibrated with the C 1s peak (BE = 284.8 eV) as criterion. Specific surface areas were measured by a nitrogen adsorption instrument (Quadrastorb SI-3MP) at 77 K after degassed at 180 °C for 6 h. The pore size distributions were determined using the Barrett-Joyner-Halenda (BJH) method.

## 2. *Electrochemical measurements*

Typically, the ink was prepared by dispersing 10 mg of samples into 500  $\mu$ L mixture containing 470  $\mu$ L ethanol and 30  $\mu$ L Nafion (5 wt %) with an ultrasonic treatment for 60 min. Then, as-made ink of all the catalysts was dropped onto Ni foam ( $1\times 1$  cm $^2$ ) to afford a loading density of 2 mg cm $^{-2}$ . After drying, the working electrodes were obtained. Electrochemical tests were carried out by using a CHI 660E electrochemical workstation with a conventional three-electrode system at room temperature, in which the sample-coated Ni foam electrode, the Ag/AgCl electrode in saturated KCl solution, and Pt wire served as the working, reference, and counter

electrode, respectively. 1 M KOH solution was used as the electrolyte.

Prior to OER and HER measurements, 1 M KOH electrolyte was saturated with high-purity O<sub>2</sub> and N<sub>2</sub>, respectively. Cyclic voltammetry (CV) was carried out at different scanning speeds (20, 40, 60, 80, 100 mV s<sup>-1</sup>) under non-faradaic potential. The electrochemical double-layer capacitance (C<sub>dl</sub>) values were obtained by a conversion method of CV curves. The linear sweep voltammetry (LSV) with 95% IR-compensation was carried out at 5 mV s<sup>-1</sup> for both OER and HER. Electrochemical impedance spectroscopy (EIS) measurements were performed in the frequency range from 100 kHz to 0.01 Hz at different applied voltages, with AC voltage amplitude of 5 mV. In addition, the current density-time (*j*-*t*) curve of optimal catalyst was also tested for evaluating stability. For overall water splitting, Ni foam loading with optimal catalyst was used as both anode and cathode electrode with a potential scan range from 1.2 to 1.9 V in home-made electrolyzer, where LSV curve with 95% IR-compensation and current density-time curve were also recorded. The potentials in OER and HER tests were converted to the reversible hydrogen electrode (RHE) potential followed by Nernst equation (1):[1]

$$E_{RHE} = E_{Ag/AgCl} + E_{Ag/AgCl}^0 + 0.059pH \quad (1)$$

The corresponding overpotential for OER and HER were obtained as equation (2) and (3): [2]

$$\eta_{OER} = E_{OER} - 1.23 V \quad (2)$$

$$\eta_{HER} = |E_{HER}| \quad (3)$$

The values of mass activity (A g<sup>-1</sup>) were calculated via the catalyst loading *m* (2

mg cm<sup>-2</sup>) and the measured current density  $j$  (mA cm<sup>-2</sup>), according to equation (4): [3]

$$\text{mass activity} = j/m \quad (4)$$

Turnover frequency (TOF) was calculated by supposing every corresponding metal atom as active sites involved with catalytic reaction, showing as equation (5): [3]

$$TOF = jS/zFn \quad (5)$$

Where  $j$  is measured current density (mA cm<sup>-2</sup>);  $S$  is geometrical surface area of working electrode (1 cm<sup>2</sup>);  $z$  is electron transfer number per molecule generated O<sub>2</sub>/H<sub>2</sub> ( $z = 4$  for OER,  $z = 2$  for HER);  $F$  is Faraday's constant (96485.3 C mol<sup>-1</sup>), and  $n$  is the moles of the corresponding metal atom (mol) within the catalyst loading.

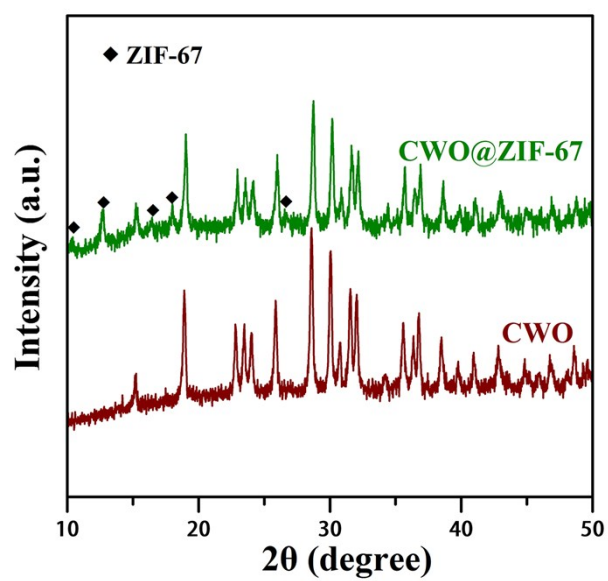


**Fig. S1** XRD patterns of as-prepared CuWO<sub>4</sub> (CWO) and CuWO<sub>4</sub>@ZIF-67 (CWO@ZIF-67) precursor.

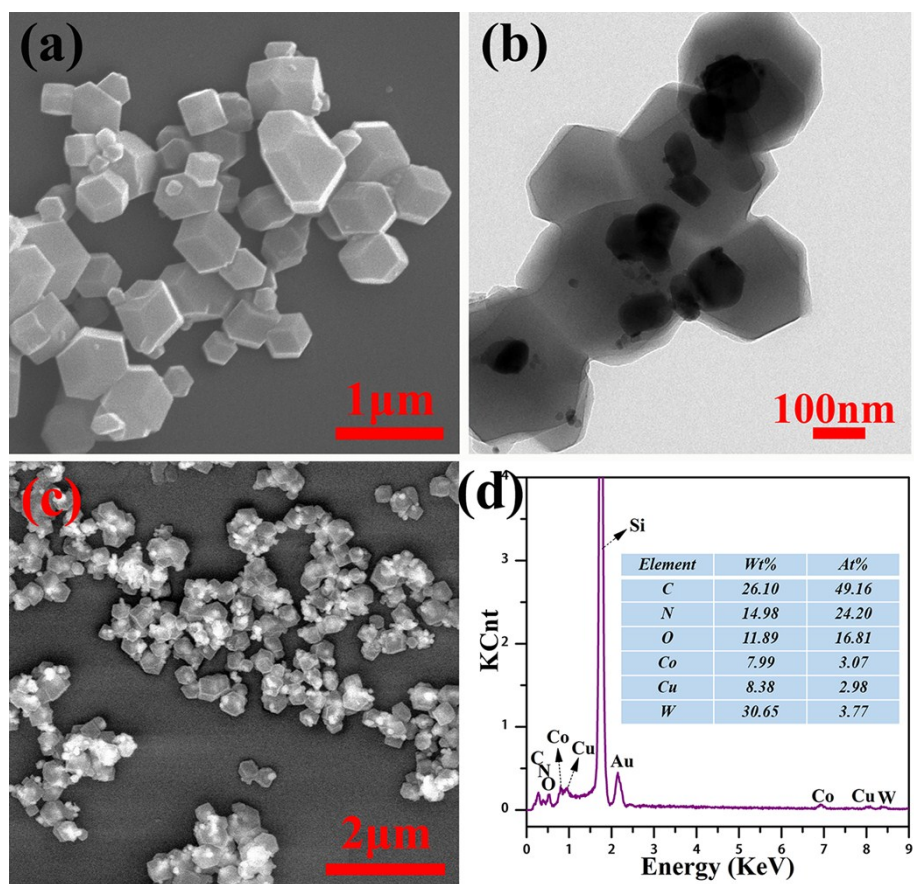


**Fig. S2** (a) SEM image, (b) TEM image, (c) BSED image, (d) SEM-EDS analysis of  $\text{CuWO}_4@\text{ZIF-67}$  precursor.

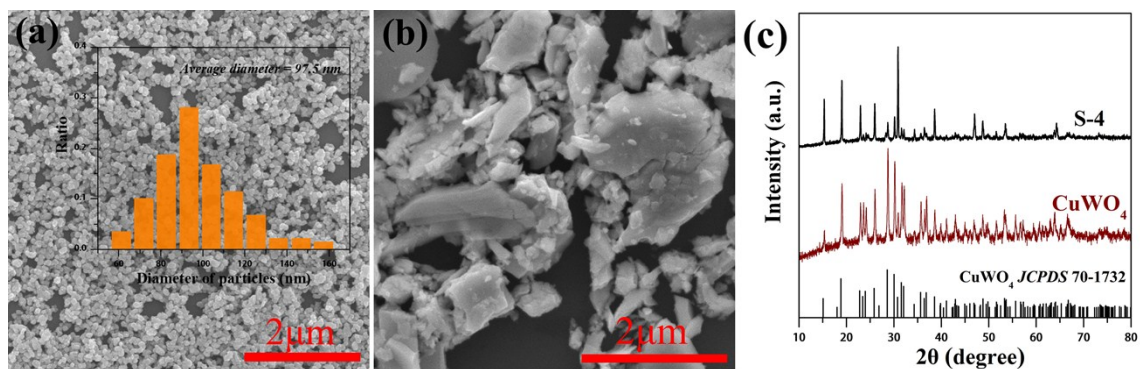


**Fig. S3** SEM image of (a) CuWO<sub>4</sub> and (b) sample S-4, (c) XRD patterns of CuWO<sub>4</sub> and sample S-4.

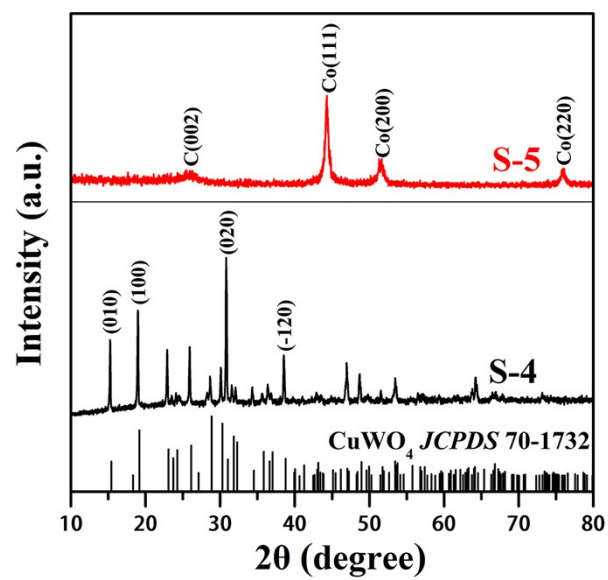


**Fig. S4** XRD patterns of as-synthesized sample S-4 and S-5.

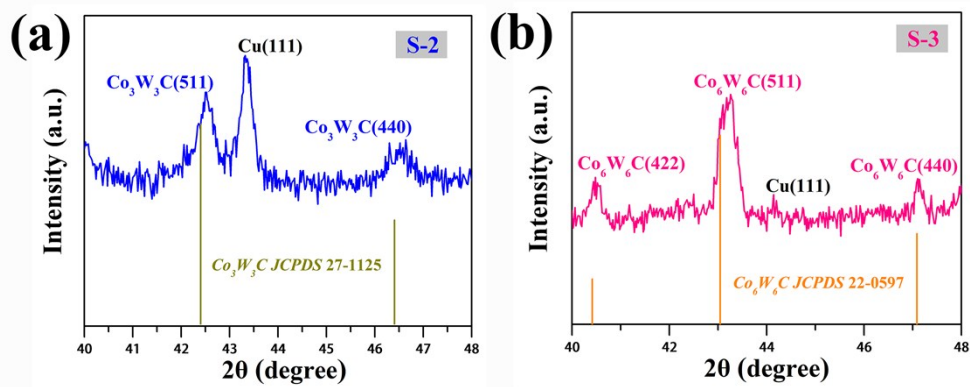


**Fig. S5** Enlarged views of corresponding XRD pattern: (a) S-2, (b) S-3.

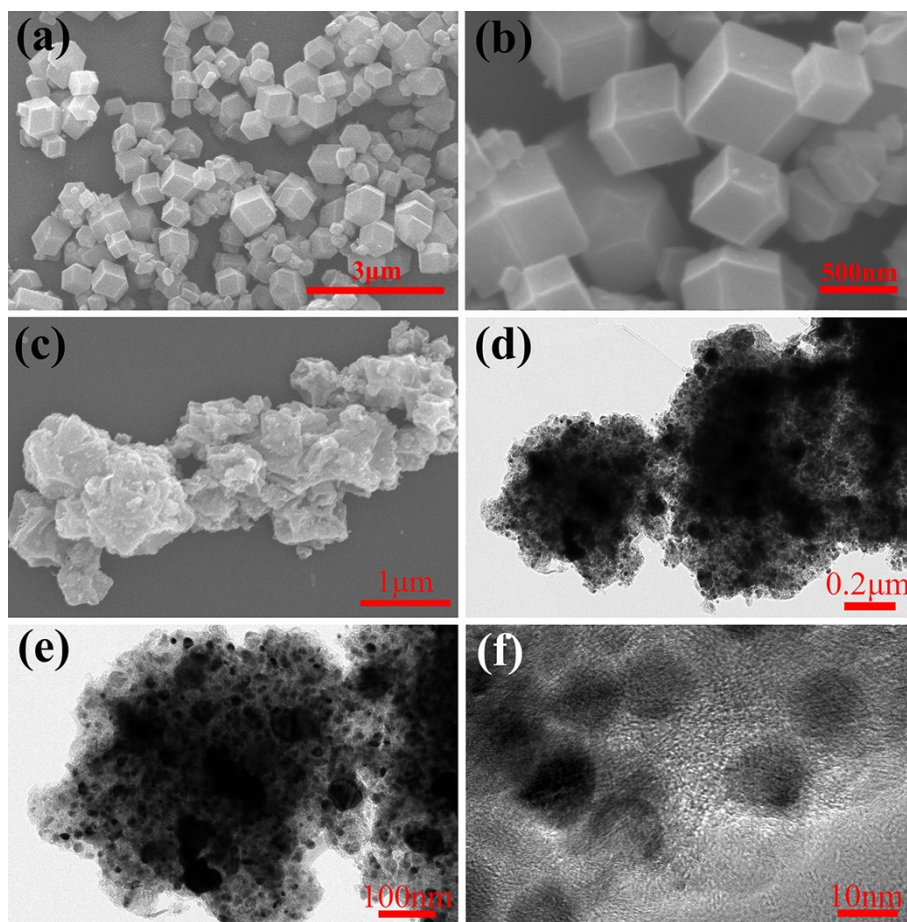


**Fig. S6** SEM images of ZIF-67 (a and b) and (c) sample S-5; (d and e) TEM images and (f) HRTEM images of as-obtained sample S-5.

**Table S1.** The relative elemental concentration in different NC@Cu-Co-W-C.

Samples	Relative Concentration (at %)				
	C	N	Cu	W	Co
S-1	70.83	17.87	2.44	2.79	6.07
S-2	68.67	3.68	7.55	11.85	8.25
S-3	66.13	2.5	13	11.53	6.84

**Table S2.** The relative concentration for different types of C in C 1s.

Samples	Relative concentration in C 1s (%)			
	C-W	C=C/C-C	C-N/C-O	O=C-O
S-1	-	62.5	24.4	13.1
S-2	0.7	71.9	17.3	10.1
S-3	6.4	71.4	12.1	10.1
Binding Energy (eV)	283.1	284.8	286.1	288.5

**Table S3.** The relative concentration for different types of N in N 1s.

<b>Samples</b>	<b>Relative concentration in N 1s (%)</b>	
	<b>Pyridinic N</b>	<b>Graphitic N</b>
<b>S-1</b>	80.6	19.4
<b>S-2</b>	43.2	56.8
<b>S-3</b>	64.9	35.1
<b>Binding Energy (eV)</b>	398.7	400.8

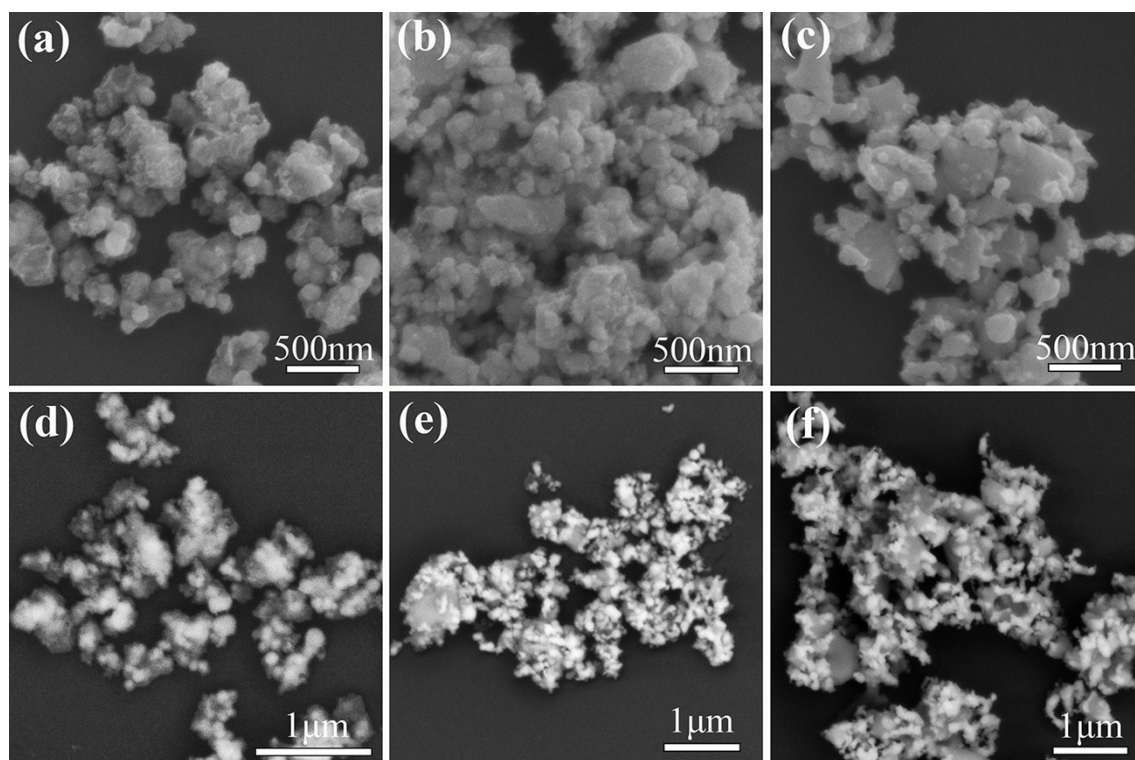


**Fig. S7** SEM images and EBSD images of NC@Cu-Co-W-C. (a and d) sample S-1, (b and e) sample S-2, (c and f) sample S-3.

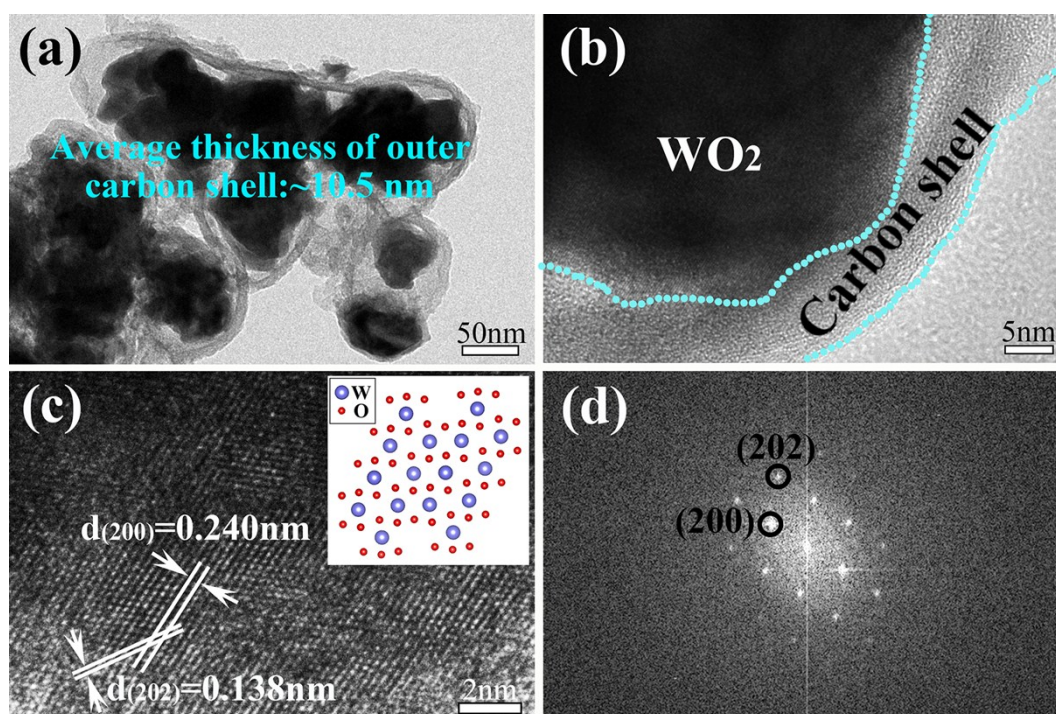


**Fig. S8** (a) TEM images; (b and c) HRTEM image, inset presents the crystal structure of WO<sub>2</sub>; (d) the corresponding FFT patterns of area (c) of S-1 sample.

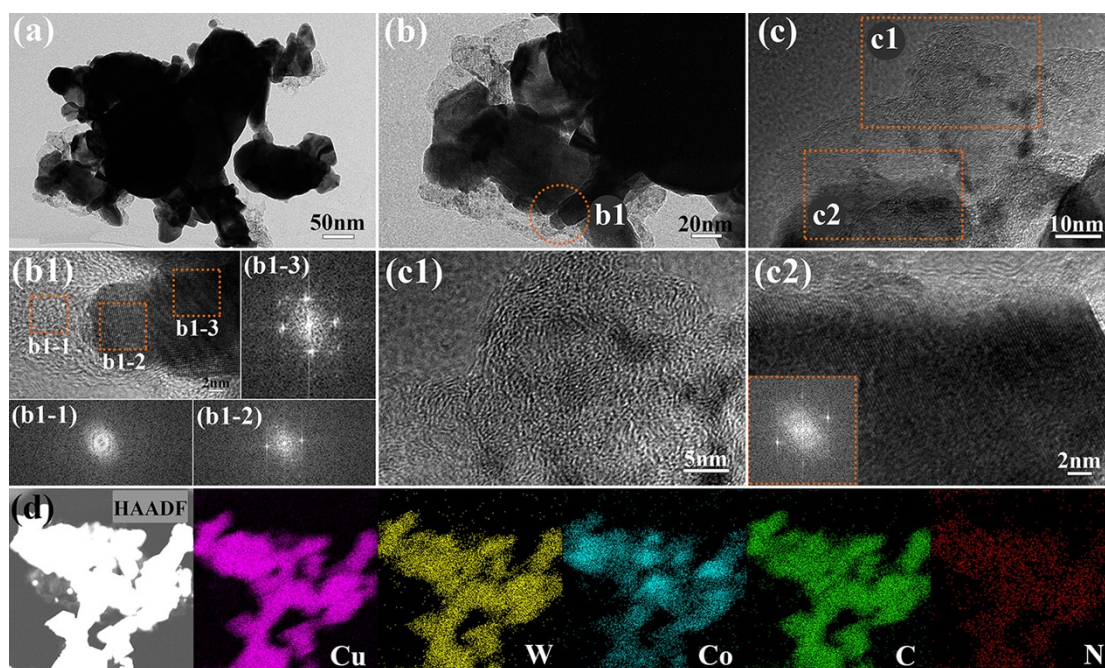


**Fig. S9** (a-c) TEM images; (b1, c1 and c2) HRTEM images and (b1-1-b1-3) the corresponding FFT patterns; (d) EDS mapping of sample S-3.

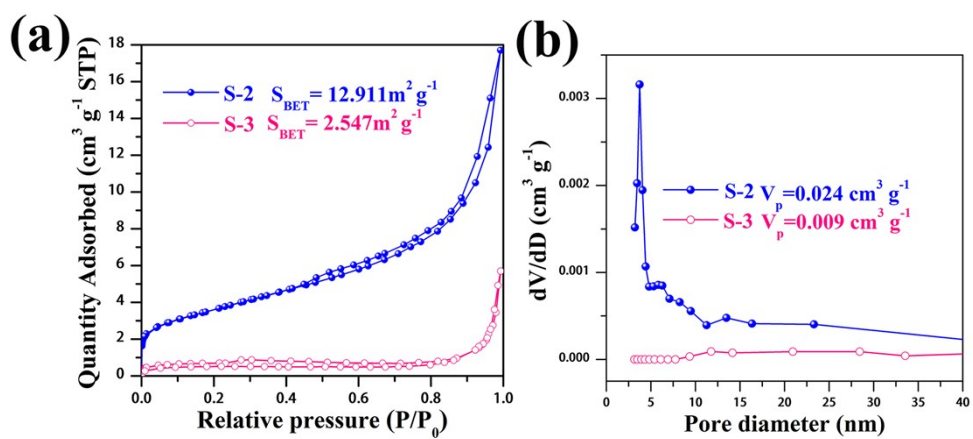


**Fig. S10** (a) N<sub>2</sub> adsorption-desorption isotherms and (b) corresponding pore size distribution of sample S-2 and S-3.

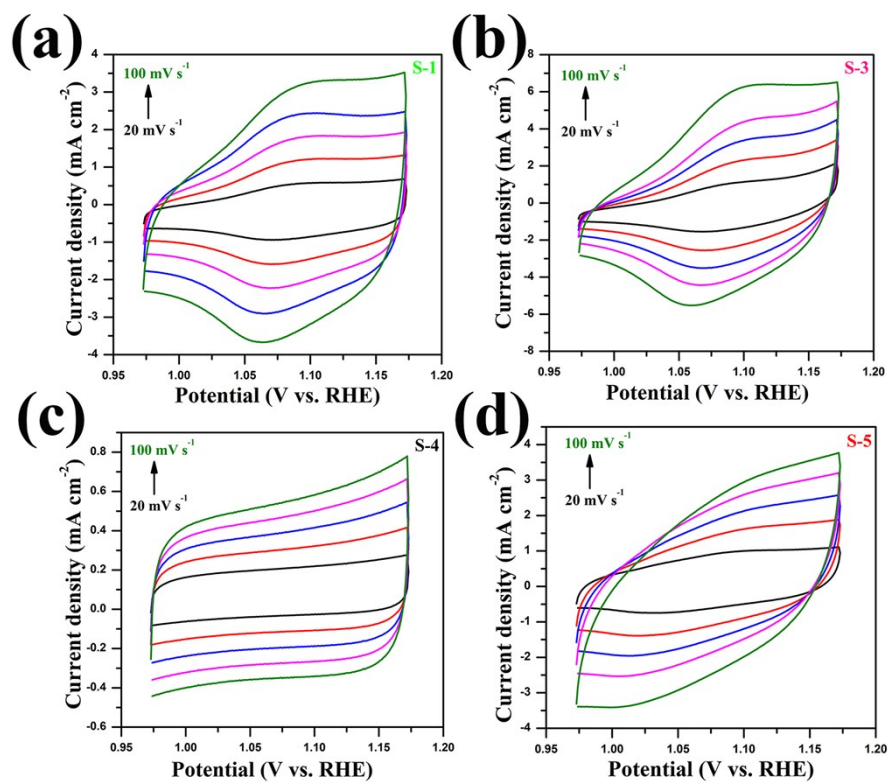


**Fig. S11** CV curves of various samples. (a) S-1, (b) S-3, (c) S-4, (d) S-5.

**Table S4** Comparison of the OER performance for NC@Cu-Co-W-C (sample S-2) catalyst and other reported metal carbide catalysts in alkaline electrolyte.

Samples	OER				Ref.
	Loading density (mg cm <sup>-2</sup> )	Electrolyte	$\eta$ (mV) at $j=10$ mA cm <sup>-2</sup>	Tafel slop (mV dec <sup>-1</sup> )	
NC@Cu-Co-W-C	2	1 M KOH	238	59	This work
Ni/Mo <sub>2</sub> C-PC	0.5	1 M KOH	368	-	[4]
Fe-Ni <sub>3</sub> C	0.15	1 M KOH	275	62	[5]
PMo/ZIF-67-6N	0.708	1 M KOH	295	39	[6]
Co <sub>6</sub> Mo <sub>6</sub> C <sub>2</sub> /NCRGO	0.14	1 M KOH	260	50	[7]
InOF-16-Ar-550	0.6	1 M NaOH	330	78	[8]
Co-Mo-C/NRGO	0.14	1 M KOH	330	42	[9]
Mo <sub>2</sub> C/Co <sub>6</sub> Mo <sub>6</sub> C <sub>2</sub> /NRGO	0.14	1 M KOH	360	50	
Co <sub>3</sub> ZnC/Co@CN	0.334	1 M KOH	366	81	[10]
0	0.28	1 M KOH	396	82	[11]
Ni-Mo <sub>x</sub> C/NC-100	0.86	1 M KOH	328	74	[12]
Ni/Ni <sub>3</sub> C	0.197	1 M KOH	350	57.6	[13]
Fe <sub>3</sub> C@NG800-0.2	0.2	1 M KOH	361	62	[14]

**Table S5** The values of charge transfer resistance ( $R_{ct}$ ) in HER and OER process for different samples.

<b>Samples</b>	<b><math>R_{ct}</math> value for OER</b>	<b><math>R_{ct}</math> value for HER</b>
<b>S-1</b>	3.32	7.59
<b>S-2</b>	2.74	5.38
<b>S-3</b>	2.72	5.64
<b>S-4</b>	60.31	10.74
<b>S-5</b>	11.16	7.77

**Table S6** Comparison of the HER performance for NC@Cu-Co-W-C (sample S-2) catalyst and other reported metal carbide catalysts.

Samples	HER				Ref.
	Loading density (mg cm <sup>-2</sup> )	Electrolyte	$\eta$ (mV) at $j=10$ mA cm <sup>-2</sup>	Tafel slop (mV dec <sup>-1</sup> )	
<b>NC@Cu-Co-W-C</b>	<b>2</b>	<b>1 M KOH</b>	<b>98</b>	<b>50</b>	<b>This work</b>
Ni/Mo <sub>2</sub> C-PC	0.5	1 M KOH	179	101	[4]
Fe-Ni <sub>3</sub> C	0.15	1 M KOH	292	41.3	[5]
PMo/ZIF-67-6-6N	0.708	1 M KOH	83	50	[6]
Mo <sub>2</sub> CT <sub>x</sub> NMs	1	1 M KOH	154	100	[15]
Co-NC@Mo <sub>2</sub> C	0.83	1 M KOH	173	65	[16]
W <sub>2</sub> C@CNT-S8	0.28	1 M KOH	148	56.2	[17]
Mo <sub>2</sub> C	2	1 M KOH	130	66.5	[18]
mC-Mo-850	0.38	1 M KOH	145	55	[19]
Zn-N-MoC-H	0.357	1 M KOH	128	52.1	[20]
Mo/Co@N-C	0.7	1 M KOH	157	148	[21]
(Mo <sub>2</sub> C) <sub>0.34</sub> -(WC) <sub>0.32</sub> -QDs/NG	0.269	1 M KOH	93	53	[22]

**Table S7** Comparison of overall water splitting performance between NC@Cu-Co-W-C (sample S-2) electrodes and other reported metal carbide catalysts electrodes.

Samples	Electrolyte	Potential at current density of 10 mA cm <sup>-2</sup> (V)	Ref.
<b>S-2//S-2</b>	<b>1 M KOH</b>	<b>1.64</b>	<b>This work</b>
Ni/Mo <sub>2</sub> C-PC//Ni/Mo <sub>2</sub> C-PC	1 M KOH	1.66	[4]
Co-NC@Mo <sub>2</sub> C// Co-NC@Mo <sub>2</sub> C	1 M KOH	1.685	[16]
Mo <sub>2</sub> C//Mo <sub>2</sub> C	1 M KOH	1.65	[18]
Co <sub>3</sub> ZnC/Co-NCCP //Co <sub>3</sub> ZnC/Co-NCCP	1 M KOH	1.65	[23]
Co <sub>9</sub> S <sub>8</sub> -NSC@Mo <sub>2</sub> C/NF// Co <sub>9</sub> S <sub>8</sub> -NSC@Mo <sub>2</sub> C/NF	1 M KOH	1.61	[24]
Co-Mo <sub>2</sub> C@NCNT/Ti// Co-Mo <sub>2</sub> C@NCNT/Ti	1 M KOH	1.628	[25]
CoP-Mo <sub>2</sub> C@NC// CoP-Mo <sub>2</sub> C@NC	1 M KOH	1.64	[26]

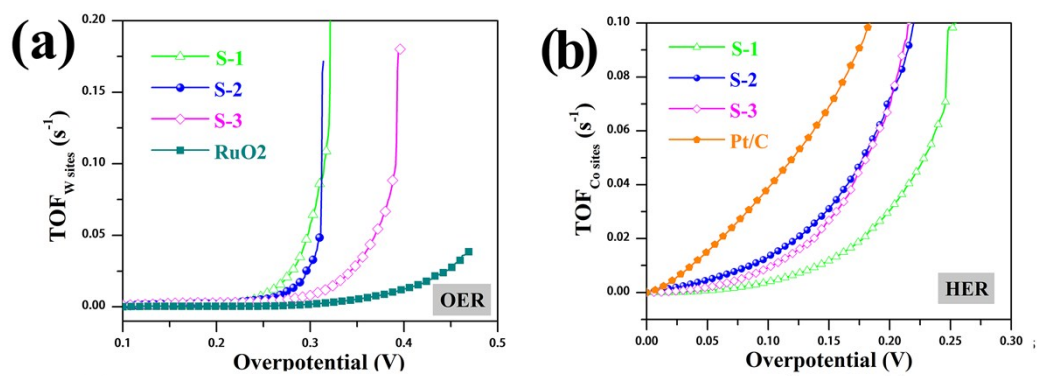


**Fig. S12** The calculated TOF values based on W active sites in OER process (a); the calculated TOF values based on Co active sites in HER process (b).

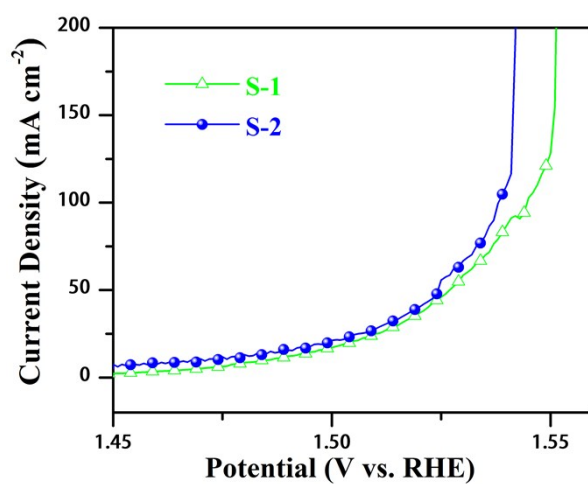


**Fig. S13** The enlarged view of OER LSV polarization curves for S-1 and S-2 sample.

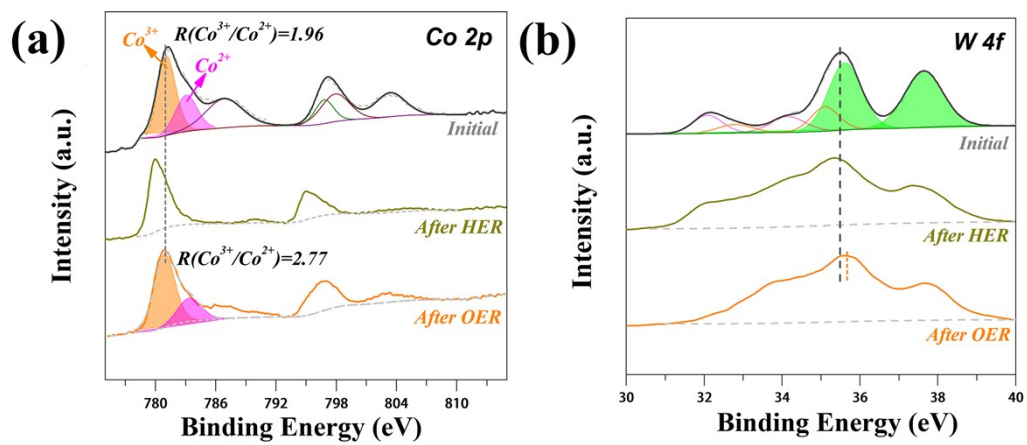


**Fig. S14** XPS spectra of the S-2 electrode before reaction, after OER, and HER stability test: (a) Co 2p, (b) W 4f.

**Table S8** A summary about HER and OER performances of different samples in 1 M KOH electrolyte.

Samples	OER				HER				$\Delta E$ between $\eta_{10}^{OER}$ and $\eta_{10}^{HER}$ (V)
	$\eta$ at j=10 mA cm <sup>-2</sup> ( $\eta_{10}^{OER}$ , mV)	Tafel slope (mV dec <sup>-1</sup> )	Mass activity (A g <sup>-1</sup> ) at $\eta=280$ mV	TOF <sub>Co</sub> (s <sup>-1</sup> ) at $\eta=280$ mV	$\eta$ at j=10 mA cm <sup>-2</sup> ( $\eta_{10}^{HER}$ , mV)	Tafel slope (mV dec <sup>-1</sup> )	Mass activity (A g <sup>-1</sup> ) at $\eta=100$ mV	TOF <sub>w</sub> (s <sup>-1</sup> ) at $\eta=100$ mV	
S-1	256	61	12.482	0.0114	137	66	2.162	0.0085	1.623
S-2	238	59	13.934	0.0176	98	50	5.181	0.0091	1.566
S-3	269	78	5.981	0.0095	125	58	2.909	0.0055	1.624
S-4	444	170	1.363	-	181	102	0.811	-	1.855
S-5	311	84	3.510	-	141	90	1.843	-	1.682
RuO <sub>2</sub>	278	87	5.324	0.0011	-	-	-	-	1.581 <sup>a</sup>
Pt/C	-	-	-	-	73	49	7.678	0.0388	

Note: (1) The “a” in “1.581<sup>a</sup>” represents the potential gap between  $\eta_{10}^{OER}$  for RuO<sub>2</sub> catalyst and  $\eta_{10}^{HER}$  for Pt/C catalyst.

(2) TOF<sub>Co</sub> means that the TOF values are calculated by supposing that Co species serve as real active sites.

## Reference

- [1]. A. Zhu, L. Qiao, P. Tan, W. Zeng, Y. Ma, R. Dong, J. Pan, *Journal of Colloid and Interface Science*, 541 (2019) 133-142.
- [2]. L. Qiao, A. Zhu, H. Yang, W. Zeng, R. Dong, P. Tan, D. Zhong, Q. Ma, J. Pan, *Inorganic Chemistry Frontiers*, 5 (2018) 2276-2283.
- [3]. M. Gao, W. Sheng, Z. Zhuang, Q. Fang, S. Gu, J. Jiang, Y. Yan, *Journal of the American Chemical Society*, 136 (2014) 7077-7084.
- [4]. Z. Y. Yu, Y. Duan, M. R. Gao, C. C. Lang, Y. R. Zheng and S. H. Yu, *Chemical Science*, 2017, **8**, 968-973.
- [5]. H. Fan, H. Yu, Y. Zhang, Y. Zheng, Y. Luo, Z. Dai, B. Li, Y. Zong and Q. Yan, *Angewandte Chemie International Edition*, 2017, **56**, 12566-12570.
- [6]. C. Chen, A. Wu, H. Yan, Y. Xiao, C. Tian and H. Fu, *Chemical Science*, 2018, **9**, 4746-4755.
- [7]. Y. J. Tang, C. H. Liu, W. Huang, X. L. Wang, L. Z. Dong, S. L. Li and Y. Q. Lan, *ACS Applied Materials & Interfaces*, 2017, **9**, 16977-16985.
- [8]. J. Qian, T. T. Li, Y. Hu and S. Huang, *Chemical Communications*, 2017, **53**, 13027-13030.
- [9]. C.-H. Liu, Y.-J. Tang, X.-L. Wang, W. Huang, S.-L. Li, L.-Z. Dong and Y.-Q. Lan, *Journal of Materials Chemistry A*, 2016, **4**, 18100-18106.
- [10]. J. Su, G. Xia, R. Li, Y. Yang, J. Chen, R. Shi, P. Jiang and Q. Chen, *Journal of Materials Chemistry A*, 2016, **4**, 9204-9212.
- [11]. X.-X. Ma, X.-Q. He and T. Asefa, *Electrochimica Acta*, 2017, **257**, 40-48.
- [12]. D. Das, S. Santra, and K. K. Nanda, *ACS Applied Materials & Interfaces*, 2018, 10, 35025–35038.
- [13]. Q. Qin, J. Hao, and W. J. Zheng, *ACS Applied Materials & Interfaces*, 2018, 10, 17827–17834.
- [14]. H. L. Jiang, Y. F. Yao, Y. H. Zhu, Y. Y. Liu, Y. H. Su, X. L. Yang, and C. Z. Li, *ACS Applied Materials & Interfaces*, 2015, 7, 21511–21520.
- [15]. Z. K. Kou, L. Zhang, Y. Y. Ma, X. M. Liu, W. J. Zang, J. Zhang, S. Z. Huang, Y. H. Du, A. K. Cheethama, J. Wang, *Applied catalysis B: Environmental*,

- 2019, 243, 678-685.
- [16]. Q. R. Liang, H. H. Jin, Z. Wang, Y. L. Xiong, S. Yuan, X. C. Zeng, D. P. He, S. C. Mu, *Nano Energy*, 2019, 57, 746-752.
- [17]. Y. Hu, B. Yu, W. X. Li, M. Ramadoss and Y. F. Chen, *Nanoscale*, 2019, 11, 4876-4884.
- [18]. J. N. Xing, Y. Li, S. W. Guo, T. Jin, H. X. Li, Y. J. Wang, L. F. Jiao, *Electrochimica Acta*, 2017, **298**, 305-312. .
- [19]. S. Li, C. Cheng, A. Sagaltchik, P. Pachfule, C. S. Zhao, and A. Thomas, *Advanced Functional Materials*, 2019, 29, 1807419.
- [20]. Q. Cao, L. L. Zhao, A. L. Wang, L. J. Yang, L. F. Lai, Z.-L. Wang, J. Kim, W. J. Zhou, Y. Yamauchi and J. J. Lin, *Nanoscale*, 2019, 11, 1700-1709.
- [21]. C. Wu, D. Liu, H. Li, and J. H. Li, *Small*, 2018, 14, 1704227.
- [22]. L. L. Huo, B. C. Liu, Z. Q. Gao and J. Zhang, *Journal of Materials Chemistry A*, 2017, 5, 18494–18501.
- [23]. Z. Yu, Y. Bai, S. M. Zhang, Y. X. Liu, N. Q. Zhang, G. H. Wang, J. H. Wei, Q. B. Wu, and K. N. Sun, *ACS Applied Materials & Interfaces*, 2018, 10, 6245–6252.
- [24]. X. H. Luo, Q. L. Zhou, S. Du, J. Li, J. W. Zhong, X. L. Deng, and Y. L. Liu, *ACS Applied Materials & Interfaces*, 2018, 10, 22291–22302.
- [25]. L. H. Ai, J. F. Su, M. Wang, and J. Jiang, *ACS Sustainable Chemistry & Engineering*, 2018, 6, 9912-9920.
- [26]. S. Dutta, A. Indra, H. S. Han, T. Song, *ChemSusChem*, 2018, 11, 3956-3964.